LETTER

Growth of graphene from solid carbon sources

Zhengzong Sun[1], Zheng Yan[1], Jun Yao[2], Elvira Beitler[1], Yu Zhu[1] & James M. Tour[1,3]

Monolayer graphene was first obtained[1] as a transferable material in 2004 and has stimulated intense activity among physicists, chemists and material scientists[1–4]. Much research has been focused on developing routes for obtaining large sheets of monolayer or bilayer graphene. This has been recently achieved by chemical vapour deposition (CVD) of CH_4 or C_2H_2 gases on copper or nickel substrates[5–7]. But CVD is limited to the use of gaseous raw materials, making it difficult to apply the technology to a wider variety of potential feedstocks. Here we demonstrate that large area, high-quality graphene with controllable thickness can be grown from different solid carbon sources—such as polymer films or small molecules—deposited on a metal catalyst substrate at temperatures as low as 800 °C. Both pristine graphene and doped graphene were grown with this one-step process using the same experimental set-up.

With its extraordinary electronic and mechanical properties, graphene is showing promise in a plethora of applications[7–13]. Graphene can now be obtained by several different approaches. The original mechanical peeling method from highly oriented pyrolytic graphite yields small amounts of high quality graphene[1]. Liquid exfoliation and reduction of graphene oxide have been used to produce chemically converted graphene in large quantities[14,15]. Annealing SiC, growth from amorphous carbon and CVD methods have been used to synthesize large-size graphene on wafers[5–7,16,17]. By introducing Ni and Cu as the substrates for CVD growth, the size, thickness and quality of the produced graphene is approaching industrially useful specifications[5–7]. However, intrinsic graphene is a zero bandgap material that shows a weak ambipolar behaviour; transistors based on such graphene show small 'on'/'off' current ratios, so they are too metallic for many designed electronics applications[18]. In order to modify the Fermi level of graphene and manipulate its electronic and optical properties, doping the graphene matrix with heteroatoms is a straightforward way to make an n-type, p-type or hybrid doped graphene[19–23].

In the present work, the growth of monolayer pristine graphene from solid carbon sources atop metal catalysts is demonstrated (Fig. 1a). The first solid carbon source used was a spin-coated poly(methyl methacrylate) (PMMA) thin film (~100 nm) and the metal catalyst substrate was a Cu film. At a temperature as low as 800 °C or as high as 1,000 °C (tested limit) for 10 min, with a reductive gas flow (H_2/Ar) and under low pressure conditions, a single uniform layer of graphene was formed on the substrate. The graphene material thus produced was successfully transferred to different substrates for further characterization (see Supplementary Materials and Supplementary Methods).

The Raman spectrum of this monolayer PMMA-derived graphene is shown in Fig. 1b and the spectrum is characteristic of >10 locations recorded over 1 cm^2 of the sample. The two most pronounced peaks in this spectrum are the G peak at 1,580 cm^{-1} and the 2D peak at 2,690 cm^{-1}. The I_{2D}/I_G intensity ratio is about 4 and the full-width at half-maximum of the 2D peak is about 30 cm^{-1}, indicating that the graphene is a monolayer. The D peak (~1,350 cm^{-1}) is in the noise level, indicating the presence of few sp^3 carbon atoms or defects[24].

The electrical properties of the PMMA-derived graphene were evaluated with back-gated graphene-based field-effect transistor (FET)

devices atop a 200-nm-thick SiO_2 dielectric. Typical data for the FET devices are shown in Fig. 1c. For this particular device, the estimated carrier (hole) mobility is ~410 $cm^2 V^{-1} s^{-1}$ at room temperature and the 'on'/'off' current ratio is ~2, which is expected in graphene-based FET devices of this size[21]. Although the graphene was pristine without any doping atoms, it still shows weak p-type behaviour, with the neutrality point moved to positive gate voltage; this probably arises from the physisorption of small molecules, such as H_2O (ref. 10). Placing graphene FETs under high vacuum (10^{-5}–10^{-6} torr) for several days moves the neutrality point to zero (Supplementary Fig. 1), confirming that the weak p-type behaviour was due to physisorption of volatile molecules[10].

Transmission electron microscopy (TEM) images of the pristine PMMA-derived graphene and its diffraction pattern are shown in Fig. 1d–g. The selected area electron diffraction (SAED) pattern in Fig. 1d displays the typical hexagonal crystalline structure of graphene. The layer count on the edges of the images indicates the thickness of this PMMA-derived graphene. The edges in Fig. 1e–g were randomly imaged under TEM and most were monolayer or bilayer graphene, which corroborates the Raman data. Although most of the graphene surface was continuous and crystalline according to its diffraction pattern, there is adsorbed PMMA resulting from the transfer step. Metal atoms or ions were also found to be trapped on the graphene surface (black arrows in Fig. 1g) and became charge impurities, which should increase the charge density but decrease the mobility of the PMMA-derived graphene[25]. Similar phenomena have been observed with CVD-generated graphene[5–7]. Atomic force microscopy was used to characterize the surface profile of PMMA-derived graphene on a SiO_2/Si substrate. In Supplementary Fig. 2, the thickness of this graphene is about 0.7 nm, which confirms the monolayer nature of this material. However, limited by the wet-transfer technique, graphene's intrinsic corrugation is still obvious in the AFM image.

Graphene's electronic properties are strongly linked to its thickness[26]. Therefore, it would be useful to be able to control the thickness when producing the graphene by tuning the growth parameters. We have found that the thickness of PMMA-derived graphene can be controlled—to give a monolayer, a bilayer, or a few layers—by changing the Ar and H_2 gas flow rate. Typical thicknesses were evaluated by Raman spectroscopy (Fig. 2a) and ultraviolet transmittance (Fig. 2b) of the graphene. At 1,000 °C, bilayer PMMA-derived graphene was obtained when the Ar flow rate was 500 cm^3 STP min^{-1} and the H_2 flow rate was 10 cm^3 STP min^{-1}. When the Ar flow rate was 500 cm^3 STP min^{-1} and the H_2 flow rate was 3–5 cm^3 STP min^{-1}, few-layer PMMA-derived graphene formed. When the H_2 flow rate was increased to 50 cm^3 STP min^{-1} or higher, only monolayer graphene was formed on the Cu substrate. Monolayer graphene showed a transmittance of 97.1% at 550 nm wavelength (Fig. 2b). It had a sheet resistance (R_s) of 1,200 Ω per square by the four-probe method, which makes it a transparent electrode material of interest. The bilayer graphene's transmittance at 550 nm wavelength is 94.3%, which shows linear enhancement in the ultraviolet absorption. The few-layer PMMA-derived graphene sheet in Fig. 2a has a transmittance of 83% at 550 nm, leading to an estimated six-layer thickness. Both the

[1]Department of Chemistry, Rice University, 6100 Main Street, Houston, Texas 77005, USA. [2]Applied Physics Program, Department of Bioengineering, Rice University, 6100 Main Street, Houston, Texas 77005, USA. [3]Richard E. Smalley Institute for Nanoscale Science and Technology, Department of Mechanical Engineering and Materials Science, Rice University, 6100 Main Street, Houston, Texas 77005, USA.
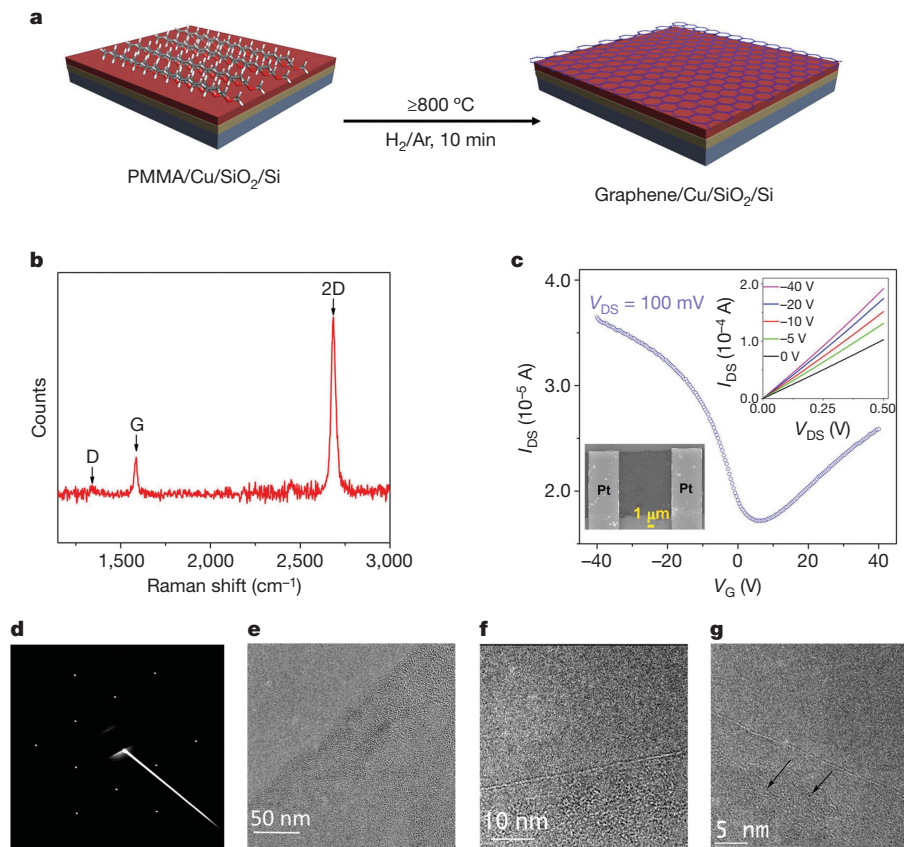
Figure 1 | Synthetic protocol, spectroscopic analysis and electrical properties of PMMA-derived graphene. a, Monolayer graphene is derived from solid PMMA films on Cu substrates by heating in an H_2/Ar atmosphere at 800 °C or higher (up to 1,000 °C). **b**, Raman spectrum (514 nm excitation) of monolayer PMMA-derived graphene obtained at 1,000 °C. See text for details. **c**, Room temperature I_{DS}–V_G curve from a PMMA-derived graphene-based back-gated FET device. Top inset, I_{DS}–V_{DS} characteristics as a function of V_G; V_G changes from 0 V (bottom) to −40 V (top). Bottom inset, SEM (JEOL-6500 microscope) image of this device where the PMMA-derived graphene is perpendicular to the Pt leads. I_{DS}, drain–source current; V_G, gate voltage; V_{DS}, drain–source voltage. **d**, SAED pattern of PMMA-derived graphene. **e–g**, HRTEM images of PMMA-derived graphene films at increasing magnification. In **g**, black arrows indicate Cu atoms.

shape and the positions of the 2D peak are significantly different from monolayer graphene to bilayer graphene and few-layer graphene (Supplementary Fig. 3). For monolayer graphene, the 2D peak can be fitted with a single sharp Lorentz peak. The observed 2D splitting in bilayer and few-layer PMMA-derived graphene can be assigned to the electronic band splitting caused by the interaction of the graphene planes[24]. The Raman mapping of the G to 2D peak ratio illustrates the uniformity of the graphene films over the 70–75 μm^2 areas investigated (Supplementary Fig. 4). For monolayer graphene, more than 95% of the film has this signature, with $I_G/I_{2D} < 0.4$. The bilayer graphene has more than 85% coverage, with an $I_G/I_{2D} \approx 0.8$.

We interpret the effect of hydrogen as follows: hydrogen acts as both the reducing reagent and a carrier gas to remove C atoms that are extruded from the decomposing PMMA during growth. A slower H_2 flow leaves more C sources for the growth of multilayer graphene. Owing to the low concentration and solubility of the carbon source in Cu, traditional CVD-grown graphene on Cu usually terminates as a monolayer. In this experiment, highly concentrated and uniformly dispersed carbon sources favour multilayer graphene when the H_2 flow is low. The higher-order layers might form through graphitization directly atop the first layer, which blocks the contact of the carbon sources with the metal catalyst. Some metal catalysts, such as Ni, are known to reverse graphene growth by converting graphene to hydrocarbon products, therefore cutting graphene along specific directions[27]. This reverse reaction does not appear to occur on the PMMA-derived graphene which is atop the Cu.

High quality monolayer PMMA-derived graphene was obtained at 800 °C by this method; this is lower than the CVD growth temperature on Cu used in the original report[6] (see Supplementary Fig. 5). For the semiconductor industry, the lower processing temperature is favourable because temperatures as high as 1,000 °C would be problematic in the fabrication of the multi-layer stacks of heterogeneous materials. Therefore, in addition to changing the Ar/H_2 flow rate, the graphene growth process was conducted at different temperatures. The quality of the graphene films was monitored by the D/G peak ratio from Raman spectroscopic analysis. The peak ratio for graphene sheets obtained at 800 °C was less than 0.1. At 750 °C, the peak ratio was ~0.35; hence 800 °C is the lower limit for obtaining high quality graphene from PMMA (Supplementary Fig. 5). We used other solid carbon sources—including fluorene ($C_{13}H_{10}$) and sucrose (table sugar, $C_{12}H_{22}O_{11}$)—to grow monolayer graphene on Cu catalyst under the same growth conditions as was used for the PMMA-derived graphene. Because these precursors are powders not films, 10 mg of each as a finely ground powder was placed directly on a 1 cm^2 Cu foil. After subjecting the powder-coated Cu films to the same reaction conditions as used for PMMA-derived graphene, Raman spectra indicated that all of the solid carbon sources were transformed into monolayer graphene with no D peak observed (Fig. 2c). Although these solid carbon precursors contain potential topological defect generators (the five-membered ring in fluorene) or high concentrations of heteroatoms (oxygen in sucrose), they produce high quality pristine graphene. It is possible that at elevated temperatures under vacuum, C has a higher affinity for the metal catalyst surface than the heteroatoms; atom rearrangement occurs and most of the topological defects are self-healed as the graphene is formed.

Other substrates—such as Ni, Si<100> with native oxide, and 200-nm-thick SiO_2 thermally grown—were also tested to determine if they
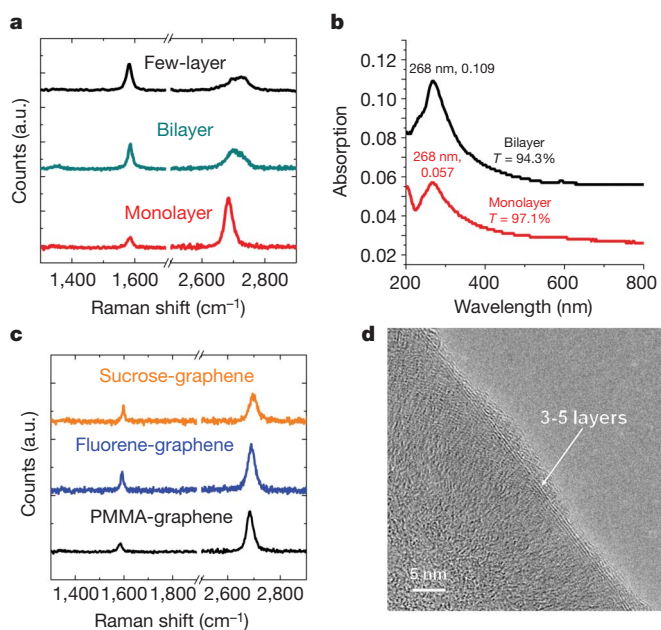
Figure 2 | Controllable growth of pristine PMMA-derived graphene films. a, Difference in Raman spectra from PMMA-derived graphene samples with controllable thicknesses derived from different flow rates of H_2. **b**, The ultraviolet–visible absorption spectra of monolayer graphene and bilayer graphene; peaks are labelled with wavelength of maximum absorption, and value of maximum absorption. The UV transmittance (T in %) is measured at 550 nm. **c**, Raman spectra of graphene derived from sucrose, fluorene and PMMA. **d**, HRTEM picture of PMMA-derived graphene grown on a Ni film. The PMMA-derived graphene was 3–5 layers thick at the edges.

would grow graphene when coated with PMMA. Figure 2d is the high-resolution TEM image of PMMA-derived graphene grown on a Ni catalyst, which clearly illustrates the few-layer structure around the edges of PMMA-derived graphene. The Raman spectra (Supplementary Fig. 6) confirm that Ni is an efficient catalytic substrate that converts PMMA into highly crystalline graphene materials with no D peak around 1,350 cm^{-1}. Under the same growth conditions, neither graphene nor amorphous carbon was obtained on Si or SiO_2 substrates, according to the Raman spectroscopic analysis of the surface after the reaction. This demonstrates the potential to grow patterned graphene from a thin film of shaped Ni or Cu deposited directly on SiO_2/Si wafers without post lithographic treatment, as PMMA-derived graphene will not grow on the Si or SiO_2 surfaces.

Pristine graphene can show weak p-type or n-type behaviour due to physisorption of small molecules, such as H_2O or NH_3 (ref. 8). However, this chemical doping effect induced by physisorption is labile, because the small molecules can be easily desorbed under heat or vacuum. Therefore, intrinsically nitrogen-doped (N-doped) graphene is more challenging to make than pristine graphene. Intrinsically N-doped graphene has been obtained by two methods: introducing a doping gas (NH_3) into the CVD systems during the graphene growth[21] or treatment of synthesized graphene or graphene oxide with NH_3 by annealing or through plasma[20,28,29]. Here, by using solid carbon sources and solid doping reagents, doped graphene can be grown in one step without any changes to the CVD system.

A doping reagent, melamine ($C_3N_6H_6$), was mixed with PMMA and spin-coated onto the Cu surface. In order to keep the nitrogen-atom concentration in the systems, we use conditions similar to those employed for the growth of PMMA-derived graphene, except that the growth was done at atmospheric pressure (Supplementary Information). The prepared polymer films were successfully converted into N-doped graphene, with an N content of 2–3.5%. The X-ray photoemission spectroscopy (XPS) data (Fig. 3a) show the difference in C 1s peaks between PMMA-derived graphene and N-doped

PMMA-derived graphene. The shoulder around 287 eV can be assigned to the C–N bonding. The N 1s peak of N-doped PMMA-derived graphene indicates that only one type of N is present, at 399.8 eV, corresponding to quaternary N in graphene[29]. This new N 1s peak also has a 4 eV shift from that in melamine, which shows an N 1s peak at 395.8 eV (Supplementary Fig. 7). The new N 1s peak suggests that the N 1s signal does not come from the melamine, but that the N atoms are uniformly bound into the graphene structure. The D peak of this material is always present in the Raman spectra, because the heteroatoms break the graphene symmetry and thereby introduce defects that are detected by Raman analysis (Fig. 3c). The D′ peak is also found in doped graphene materials obtained by the other doping methods[22,28]. The 2D peak position and I_{2D}/I_G intensity ratio reveal that this N-doped PMMA-derived graphene is monolayer graphene. Compared to PMMA-derived graphene, the I_{2D}/I_G ratio decreased from 4 to 2, implying a successful doping, according to the previously reported electrostatically gated Raman results[30].

Doping effects were also demonstrated by FETs based on N-doped PMMA-derived graphene. The n-type behaviour shown in Fig. 3d, with the neutrality point shifted to negative gate voltage, is consistently observed for devices on the same piece of N-doped PMMA-derived graphene. After keeping these FET devices under vacuum (10^{-5}–10^{-6} torr) for 24 h, their neutrality point did not move to 0 V, indicative of the covalent bonding between carbon and nitrogen rather than just physisorption; the dopant N atoms donate free electrons to graphene. Meanwhile, the mobility of N-doped graphene calculated from the N-doped FETs was about two orders of magnitude lower than in PMMA-derived graphene[21]. Owing to the broken symmetry of the lattice structure of the N-doped graphene, the N atoms act as scattering centres that suppress its mobility[26]. Patterned hydrogenation on graphene already shows its bandgap opening[31]. Similarly, if the doping atoms are periodically dispersed in graphene's matrix, they can not only
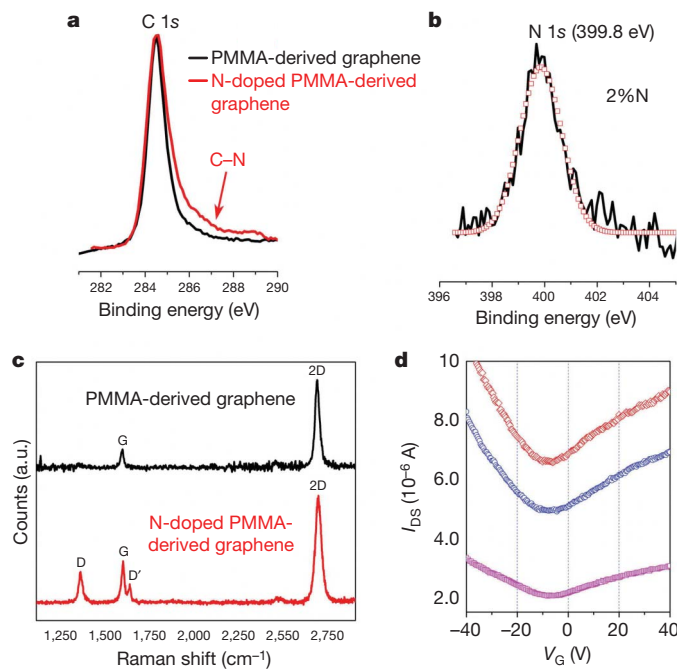
Figure 3 | Spectroscopic analysis and electrical properties of pristine and N-doped PMMA-derived graphene. a, XPS analysis from the C 1s peak of PMMA-derived graphene (black) and N-doped PMMA-derived graphene (red); the shoulder can be assigned to the C–N bond. **b**, XPS analysis, showing the N 1s peak (black line) and its fitting (squares), of N-doped PMMA-derived graphene. The atomic concentration of N for this sample is about 2% (C is 98%). No N 1s peak was observed for pristine PMMA-derived graphene. **c**, Raman spectra of pristine and N-doped PMMA-derived graphene. **d**, Room temperature I_{DS}–V_G curves ($V_{DS} = 500$ mV) showing n-type behaviour obtained from three different N-doped graphene-based back-gated FET devices.

tune the Fermi level of graphene, but also tailor its bandgap. However, in the present N-doped graphene, the 'on'/'off' current ratio does not increase, which suggests that the N atoms are randomly incorporated into the graphene matrix. In order to manipulate both the Fermi level and the bandgap of graphene, patterned doping has to be achieved[31].

In conclusion, we have demonstrated a one-step method for the controllable growth of both pristine graphene and doped graphene using solid carbon sources. This stands as a complementary method to CVD growth while permitting growth at lower temperature.

METHODS SUMMARY

Raman spectroscopy was performed on transferred graphene films on 100 nm SiO_2/Si wafers with a Renishaw Raman microscope using 514-nm laser excitation at room temperature. The electrical properties were measured in a probe station (Desert Cryogenic TT-probe 6 system) under vacuum (10^{-5}–10^{-6} torr). The I–V data were collected by an Agilent 4155C semiconductor parameter analyser. The high-resolution TEM images were taken using a 2100F field emission gun transmission electron microscope with graphene samples directly transferred onto a C-flat TEM grid (Protochips). XPS was performed on a PHI Quantera SXM scanning X-ray microprobe with 45° takeoff angle and 100 μm beam size.

1. Novoselov, K. S. *et al.* Electric field effect in atomically thin carbon films. *Science* **306,** 666–669 (2004).
2. Geim, A. K. & Novoselov, K. S. The rise of graphene. *Nature Mater.* **6,** 183–191 (2007).
3. Novoselov, K. S. *et al.* Two-dimensional gas of massless Dirac fermions in graphene. *Nature* **438,** 197–200 (2005).
4. Ruoff, R. S. Graphene: Calling all chemists. *Nature Nanotechnol.* **3,** 10–11 (2008).
5. Reina, A. *et al.* Large area, few-layer graphene films on arbitrary substrates by chemical vapor deposition. *Nano Lett.* **9,** 30–35 (2009).
6. Li, X. *et al.* Large-area synthesis of high-quality and uniform graphene films on copper foils. *Science* **324,** 1312–1314 (2009).
7. Kim, K. S. *et al.* Large-scale pattern growth of graphene films for stretchable transparent electrodes. *Nature* **457,** 706–710 (2009).
8. Lin, Y. *et al.* Operation of graphene transistors at gigahertz frequencies. *Nano Lett.* **9,** 422–426 (2009).
9. Lin, Y. *et al.* 100-GHz transistors from wafer-scale epitaxial graphene. *Science* **327,** 662 (2010).
10. Schedin, F. *et al.* Detection of individual gas molecules adsorbed on graphene. *Nature Mater.* **6,** 652–655 (2007).
11. Stankovich, S. *et al.* Graphene-based composite materials. *Nature* **442,** 282–286 (2006).
12. Stoller, M. D. *et al.* Graphene-based ultracapacitors. *Nano Lett.* **8,** 3498–3502 (2008).
13. Schlapbach, L. & Züttel, A. Hydrogen-storage materials for mobile applications. *Nature* **414,** 353–358 (2001).
14. Hernandez, Y. *et al.* High-yield production of graphene by liquid-phase exfoliation of graphite. *Nature Nanotechnol.* **3,** 563–568 (2008).
15. Stankovich, S. *et al.* Synthesis of graphene-based nanosheets via chemical reduction of exfoliated graphene oxide. *Carbon* **45,** 1558–1565 (2007).
16. Berger, C. *et al.* Electronic confinement and coherence in patterned epitaxial graphene. *Science* **312,** 1191–1196 (2006).
17. Zheng, M. *et al.* Metal-catalyzed crystallization of amorphous carbon to graphene. *Appl. Phys. Lett.* **96,** 063110 (2010).
18. Li, X. *et al.* Chemically derived, ultrasmooth graphene nanoribbon semiconductors. *Science* **319,** 1229–1232 (2008).
19. Panchakarla, L. S. *et al.* Synthesis, structure, and properties of boron- and nitrogen-doped graphene. *Adv. Mater.* **21,** 4726–4730 (2009).
20. Wang, X. *et al.* N-doping of graphene through electrothermal reactions with ammonia. *Science* **324,** 768–771 (2009).
21. Wei, D. *et al.* Synthesis of N-doped graphene by chemical vapor deposition and its electrical properties. *Nano Lett.* **9,** 1752–1758 (2009).
22. Ci, L. *et al.* Atomic layer of hybridized boron nitride and graphene domains. *Nature Mater.* **9,** 430–435 (2010).
23. Rao, C. N. R. *et al.* Some novel attributes of graphene. *J. Phys. Chem. Lett* **1,** 572–580 (2010).
24. Ferrari, A. C. *et al.* Raman spectrum of graphene and graphene layers. *Phys. Rev. Lett.* **97,** 187401–187404 (2006).
25. Chen, J. H. *et al.* Charge-impurity scattering in graphene. *Nature Phys.* **4,** 377–381 (2008).
26. Zhang, Y. *et al.* Direct observation of widely tunable bandgap in bilayer graphene. *Nature* **459,** 820–823 (2009).
27. Ci, L. *et al.* Controlled nanocutting of graphene. *Nano Res.* **1,** 116–122 (2008).
28. Lin, Y. *et al.* Controllable graphene N-doping with ammonia plasma. *Appl. Phys. Lett.* **96,** 133110 (2010).
29. Li, X. *et al.* Simultaneous nitrogen doping and reduction of graphene oxide. *J. Am. Chem. Soc.* **131,** 15939–15944 (2009).
30. Das, A. *et al.* Monitoring dopants by Raman scattering in an electrochemically top-gated graphene transistor. *Nature Nanotechnol.* **3,** 210–215 (2008).
31. Balog, R. *et al.* Bandgap opening in graphene induced by patterned hydrogen adsorption. *Nature Mater.* **9,** 315–319 (2010).

Author Contributions Z.S. designed the experiments, discovered the procedures for graphene growth, performed the spectroscopic characterizations and analysis and wrote the manuscript. Z.Y. optimized the growth conditions and contributed to the spectroscopic characterizations. J.Y. performed the electrical measurements and analysis. E.B. contributed to the electrical measurements and analysis. Y.Z. carried out the sheet resistance and transmittance measurements. J.M.T oversaw all research phases and revised the manuscript. All authors discussed and commented on the manuscript.

Author Information Reprints and permissions information is available at www.nature.com/reprints. The authors declare no competing financial interests. Readers are welcome to comment on the online version of this article at www.nature.com/nature. Correspondence and requests for materials should be addressed to J.M.T. (tour@rice.edu).